JOURNAL OF Materials CHEMISTRY

Self-assembly of gold nanoclusters on micro- and nanoelectronic substrates

Arthur W. Snow,* Mario G. Ancona, Walter Kruppa, Glenn G. Jernigan, Edward E. Foos and Doe Park

Naval Research Laboratory, Washington DC 20375, USA. E-mail: snow@ccf.nrl.navy.mil

Received 1st October 2001, Accepted 2nd January 2002
First published as an Advance Article on the web 18th February 2002

Layer-by-layer self-assembly of hexanethiol stabilized gold nanoclusters by a series of alkanedithiol coupling agents [$HS(CH_2)_nSH$, $n = 6, 8, 9, 12$] onto SiO_2/Si substrates with micron- and nanometre-scale Au electrodes is investigated by electron transport and XPS measurements. The self-assembly process for each layer consists of a two-step cycle of alkanedithiol treatment and gold cluster deposition. For maximized electron transport, critical features to optimize are the alkanedithiol chain length and the extent of dithiol coupling agent displacement of the hexanethiol ligand. Substitution of a phenethyl for the hexyl structure in the cluster ligand shell significantly enhances conductivity while substitution of a phenylene structure in the dithiol coupling agent has little effect on electron transport. Current–voltage characteristics for self-assembled depositions on the micron-scale electrode are found to be ohmic whereas *I–V* characteristics for analogous self-assemblies on the nanometre-scale electrode are initially nonlinear but become increasingly ohmic after about 3 cycles of deposition. The nonlinear features observed at the nanoscale are believed to be associated with Coulomb blockade.

Introduction

It seems self-evident that if an electronics based on molecules or nanoclusters is ever to be realized, its first applications will be as hybrids formed in combination with conventional silicon technology. An example of such an application is nanocluster-based chemical sensors.[1] Whether this line of development can then go on to impact the impending "scaling crisis" in mainstream, high-density electronics technology is of course much less clear. But under any circumstance if molecular/nanocluster-based electronics is to be pursued it is essential that one have a thorough understanding of the chemistry of deposition of molecular/nanocluster components on conventional substrates. This goal is the chief motivation of the present paper which focuses on the chemical self-assembly of gold nanoclusters onto microelectronic substrates and on how the electron transport through the nanocluster deposition depends on details of the self-assembly process.

Gold nanoclusters have a number of attractive properties that have led to their receiving significant attention over a number of years. From a chemical viewpoint they are relatively simple, being easily synthesized, stored, manipulated and functionalized. From the standpoint of electronics they are also quite simple as compared with other possible electronic "components" at the nanoscale such as molecules, semiconductor clusters or nanotubes. In particular, their electronic properties are dominated by their ultra-small sizes (diameters down to 0.7 nm) which imply large Coulomb energies (as big as 0.75 eV) and hence the possibility of Coulomb blockade effects at room temperature. The work that first generated interest in gold nanoclusters for electronics was STM measurements of single clusters sitting on planar gold substrates.[2] In this configuration, clear Coulomb staircase *I–V* characteristics have been observed[3] as have the effects of changing the cluster size[4] and the pH of a surrounding fluid (chemical gating).[5] These results, while physically interesting and very intriguing, are impractical because of their use of the STM and because of the difficulty of providing a third terminal. For these reasons we view a lateral configuration where gold clusters are interposed between two laterally separated electrodes as being of most interest.

Cluster devices configured in a lateral geometry have been studied by a number of groups[6] and fabrication of nanoparticle architectures for electronic applications has been the subject of a recent review.[7] In our research we have focused on using ultra-small clusters and on applications to both electronic devices[8] and chemical sensors.[1a] With respect to electronics applications the interest is in devices with nanoscale electrodes fabricated by e-beam lithography and with at most a few layers of clusters. These devices, of which a typical example is shown in the SEM picture in Fig. 1A, have gap spacings of 12–100 nm and show strongly nonlinear *I–V* characteristics as a result of the Coulomb blockade.[8a] With respect to chemical sensing, chemiresistor vapor sensors have used micron-scale interdigital electrodes for the past 20 years.[9] A micrograph of this device is depicted in Fig. 1B. These devices typically have numerous ($\sim$50) "finger pairs" extending from parallel contact pads and separated by micron scale gaps. When coated with a film of metal clusters, this device displays ohmic *I–V* characteristics[10] because of the statistical averaging that occurs over the large numbers of parallel current paths.

The subject matter of this paper is therefore the chemistry of self-assembly of single and multiple layer films of gold nanoclusters formed on insulating substrates and with contact to gold electrodes at both micron and nano-scales (Fig. 1). This process is found to be very sensitive to the molecular character of both the cluster and the coupling agent as well as the conditions of the deposition. This is particularly important when a selective and quantitative deposition of clusters is desired along with particular electrical properties. Among the issues addressed are the time dependence of the self-assembly deposition, the deposition's selectivity for gold surfaces, the role of the dithiol coupling agent in the deposition process and in consequent electron transport, and the reversibility of the deposition.

 DOI: 10.1039/b108859a

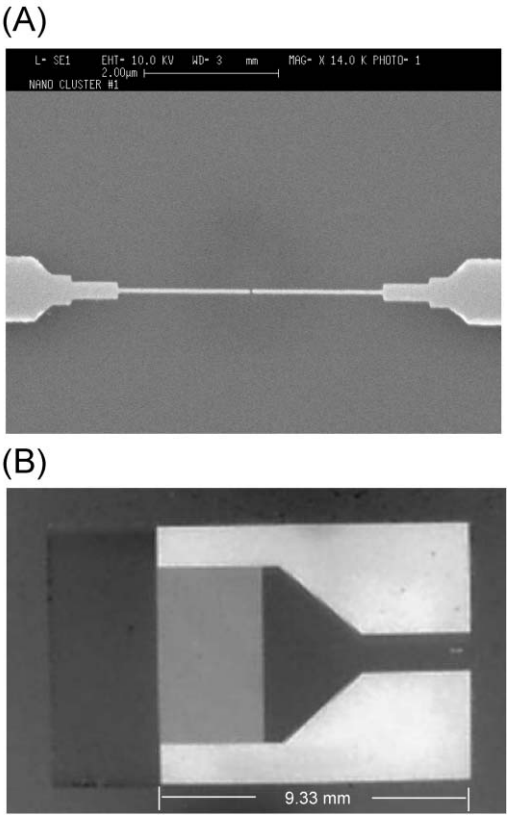

Fig. 1 Micrographs of the nano-scale (A) and micron-scale (B) electrodes.

Experimental

General information

All reagents and solvents were of reagent-grade quality, purchased commercially, and used without further purification unless otherwise noted.

Synthesis of Au : C_6(1 : 1) cluster

The synthesis procedure parallels that reported by Brust *et al.*[11] The following solutions were prepared in acid cleaned glassware: 4.56 g (8.34 mmol) $(nC_8H_{17})_4NBr$ in 167 ml toluene; 0.751 g (1.91 mmol) $HAuCl_4 \cdot 3H_2O$ in 63 ml 3 × distilled water; 0.224 g (1.89 mmol) $nC_6H_{13}SH$ in 1 ml toluene; 0.791 g (20.9 mmol) $NaBH_4$ in 52.5 ml 3 × distilled water. To the $(nC_8H_{17})_4NBr$–toluene solution in a 500 ml Erlenmeyer reaction flask was added the $HAuCl_4$–H_2O solution with rapid stirring. After 2 min the $C_6H_{13}SH$–toluene solution was transferred to the reaction flask with continued rapid stirring. The $NaBH_4$–H_2O solution was added to the reaction flask with very rapid stirring over a 30 s period. Very rapid stirring was continued for 3 h. The reaction was worked up by separation of the toluene phase and rotary evaporation of the toluene (55 °C, 60 Torr) to a 10 ml volume. This concentrated solution was added dropwise to 400 ml rapidly stirred methanol to precipitate the crude product. The product was collected by centrifugation and vacuum dried. The crude product was dissolved in 6 ml pentane and reprecipitated by dropwise addition into 200 ml of rapidly stirred methanol. After settling for 1 h, the product was collected by centrifugation and vacuum dried. Yield 0.409 g. IR (neat/cm^{-1}) 2956, 2921, 2851, 1458, 1255, 723. NMR (4.9% w/w $CDCl_3$): ^1H (δ ppm, TMS) 0.89 br, 1.30 br; ^{13}C (δ ppm, TMS) 14.2 br, 22.8 br, 33.5 br. TGA (N_2 atm, 600 °C) 82.4% w/w residual gold.

Synthesis of Au : C_2C_6(1 : 1) cluster

This procedure also parallels that reported by Brust *et al*[11] for this particular type of cluster[12] and follows the general procedure above for the Au : C_6(1 : 1) cluster. A solution of 9.12 g (16.7 mmol) $(nC_8H_{17})_4NBr$ in 334 ml toluene was mixed with 1.656 g (4.20 mmol) $HAuCl_4 \cdot 3H_2O$ in 125 ml water and 0.582 g (4.21 mmol) $C_6H_5CH_2CH_2SH$ in 2 ml toluene, then reacted with 1.60 g (43.2 mmol) $NaBH_4$ in 105 ml water. The crude product was dissolved in 5 ml toluene and reprecipitated by dropwise addition into 400 ml of rapidly stirred methanol. After settling overnight at −20 °C, the product was collected by centrifugation and vacuum dried. Yield 0.934 g. IR (neat/cm^{-1}) 3060, 3027, 2923, 2852, 1602, 1495, 1452, 1304, 1260, 1030, 748, 696. NMR (4.8%w/w $CDCl_3$): ^1H (δ ppm, TMS) 3.0 br, 7.0 br; ^{13}C (δ ppm, TMS) 126 br, 128.5 br. TGA (N_2 atm, 600 °C) 82.6% w/w residual gold.

Synthesis of dodecane-1,12-dithiol

Conversion of alkyl bromide to thiol *via* thiourea adduct formation and subsequent hydrolysis procedures were utilized.[13] To a 25 ml flask fitted with a stirring bar, condenser and nitrogen inlet were added 3.00 g (9.14 mmol) dodecane-1,12-diyl dibromide, 1.41 g (18.5 mmol) thiourea, 7.0 ml ethanol and 0.4 g water. This solution was refluxed under nitrogen for 3 h. Then 10 ml of a 10% NaOH–water solution was added and reflux continued for 3 more hours. On cooling approximately 0.5 ml oil formed and was separated. The aqueous phase was concentrated by rotary evaporation (50 °C, 20 Torr) to an approximate 5–6 ml volume. This was neutralized by dropwise addition of conc. HCl and extracted 2 × with 10 ml CH_2Cl_2. The CH_2Cl_2 extracts were combined with the separated oil, back extracted with 10 ml water, dried over anh. Na_2SO_4, filtered, evaporated to dryness and vacuum dried yielding a colorless oil that crystallized on standing (1.91 g, 89.1%). Characterization: mp 30.5 °C; ^1H NMR (300 MHz, 5.0% (w/w) $CDCl_3$) δ 2.49 (quartet, 2H, S-CH_2-), 1.58 (quintet, 2H, S-CH_2-CH_2-), 1.30 (t, H-S-), 1.4–1.2 (broad multiplet, 9H); ^{13}C NMR (75.5 MHz, 6.3% (w/w) $CDCl_3$) δ 33.97, 29.47, 29.43, 28.99, 28.29, 24.58; IR (neat) ν 2922 (s, CH_2), 2849 (s, CH_2), 2560 (w, SH), 1466, 719 cm^{-1}; *m/z* 232, 233, 234.

Cluster self-assembly procedure onto interdigital microelectrode

This electrode/substrate (Microsensor Systems, Inc. P/N 302) is a gold electrode array fabricated on a 7.3 × 12.3 × 0.42 mm quartz substrate (Fig. 1b). The electrode consists of 50 finger pairs with the following dimensions: spacing, 15 μm; overlap length, 4800 μm; electrode thickness; 1500 Å. Immediately prior to deposition, this device is cleaned by washing in $CHCl_3$, 2 min immersion in 3% NaOH–water, two-stage rinse in 3 × distilled water, vacuum drying and plasma treating in a low vacuum (three successive 5 s admissions of 20% oxygen in nitrogen at 1 Torr followed by pump down to 0.1 Torr or less). This cleaning is immediately followed by the first cycle of the self-assembly deposition which consists of three 15 min immersion steps in thiol solutions and one 15 min immersion in the cluster solution. The substrate is first immersed in a 1.0% w/w alkanedithiol–$CHCl_3$ solution (to functionalize the gold electrode surface) followed by a two-stage immersion in clean $CHCl_3$. The second step is an immersion in a 5.0% w/w (3-mercaptopropyl)trimethoxysilane–heptane solution (to functionalize the SiO_2 surface between the electrodes) followed by a two-stage immersion in clean heptane. The third step is a re-immersion in the 1.0% w/w alkanedithiol–$CHCl_3$ solution (to displace any (3-mercaptopropyl)trimethoxysilane that may have bonded to the electrode surface by displacing the alkanedithiol from the first step) followed again by a two-stage immersion in clean $CHCl_3$. The device is then immersed in a 0.50% w/w Au : C_6(1 : 1) (or Au : C_2C_6(1 : 1)) cluster–$CHCl_3$

solution followed by washing with the two-stage immersion in clean $CHCl_3$. Successive cycles of deposition consist of 2 min alternate immersions in the alkanedithiol and gold cluster solutions with the two-stage solvent washing between each immersion.

Electrical measurements using the interdigital microelectrode

A contact template (35 × 7.5 × 1.6 mm) was fashioned from an epoxy circuit board with pressure clip contacts and connecting lead wires soldered to one end. The electrode substrate slides into the template which is in turn enclosed in a 10 × 75 mm tube for air current shielding and possibly for providing a controlled atmosphere. Current is measured using a Keithley Model 617 Programmable Electrometer at a constant bias of 50 mV.

Cluster self-assembly procedure onto SiO_2 coated wafers and nanoelectrodes

The substrate is a silicon wafer covered with a layer of SiO_2. The nanoelectrodes consist of an end-on finger pair patterned by e-beam lithography at NRL (Fig. 1a). These electrodes are gold over chromium with widths and thicknesses of 50 and 30 nm, respectively. The spacing between the fingers ranges from 12 to 160 nm. This device is cleaned by 10 min immersion in a freshly prepared and boiling solution of 1 : 1 : 3 concentrated NH_4OH : 30% H_2O_2 : 3× distilled water immediately prior to the self-assembly of the cluster films. The self-assembly process is identical to that used on the micron electrodes.

Electrical measurements using the nanoelectrode

The electrical measurements on the nanoelectrode devices were performed using a micro-manipulated cryoprobe system (Janis CT-420) that allows electrical measurements to be made without special packaging down to 5 K.

XPS measurements

X-Ray photoelectron spectroscopy (XPS) measurements were made in a Vacuum Generators ESCALab MKII instrument, which consists of a dual anode X-ray source, a hemispherical analyzer, and a sample stage with multi-axial adjustability. 300 W Mg X-rays ($h\nu$ = 1253.6 eV) were used to excite photoelectrons from Au 4f, Si 2p, Cl 2p, S 2p, C 1s and O 1s core levels, which were then collected using a 50 eV pass energy. A special platen was used to hold up to 8 samples thereby permitting the analysis of multiple samples and references to assure uniformity and consistency in the data.

Results and discussion

Chemical system design

The clusters used in this work consist of a gold core stabilized by an encapsulating monolayer of alkanethiol. These clusters are synthesized by the reduction of $HAuCl_4$ with $NaBH_4$ in the presence of an alkanethiol.[11] The diameter of the core is determined by the gold to alkanethiol reagent stoichiometry, and the thickness of the alkanethiol monolayer shell is determined by the molecular dimensions of the alkanethiol.[10] The clusters are designated as $Au:C_6(1:1)$ and $Au:C_2C_6$ (1 : 1) which correlate with 1 : 1 Au : thiol reagent molar ratios and with ligand shells composed of hexanethiol and phenylethanethiol respectively. The $Au:C_6(1:1)$ cluster has a core diameter of 1.8 nm and a ligand shell thickness is 0.5 nm. The $Au:C_2C_6(1:1)$ cluster is similar in dimensions and bonding at the gold core but is different in chemical and rheological aspects. While there are 6 carbon atoms from the sulfur linkage to the extremity of the hexanethiol, the phenylethanethiol ligand molecule has the rigidity and polarizability of an aromatic structure. As such, differences in molecular chain flexibility and chemical interactions within the ligand shell of these two clusters may have important implications for both the self-assembly of and electron transport through films of these clusters.

The self-assembly chemistry used to deposit monolayer encapsulated gold clusters onto a gold electrode surface is depicted in Fig. 2. A monolayer of an alkane-α,ω-dithiol is first adsorbed onto the gold electrode leaving free terminal thiol groups oriented away from the surface. The gold cluster is then immobilized onto the surface by a ligand displacement reaction wherein the free terminal thiol of the dithiol in the adsorbed monolayer bonds to the gold core surface by displacing a monofunctional alkanethiol of the cluster ligand shell. When successive monolayers of clusters are deposited onto the initial one by alternate immersion treatments in solutions of alkanedithiol and gold clusters, the alkanedithiol becomes a coupling agent between clusters. This gold cluster self-assembled deposition chemistry is very similar to that described by Bethell *et al.*[14] and later by others[15] with the exception that in our case the cluster is initially encapsulated by a monolayer of monofunctional alkanethiol. A consequence of this difference is that much of the initially-present monofunctional alkanethiol is retained in the individual clusters shells of the deposition. An advantage is that greater control over core size and dispersity can thereby be exercised since the dimensions of the monolayer encapsulated clusters can be regulated by the Au : alkanethiol molar ratio in their syntheses,[10] and they are sufficiently stable to undergo fractionation operations such as size exclusion chromatography[11] or solvent fractionation.[16] When synthesized without the alkanethiol monolayer, the clusters are much larger in size and irreversibly aggregate on solvent removal.[14] Also, gold clusters without a protective monolayer or with only a very thin ligand shell have a nonspecific adsorption, particularly on silicon oxide surfaces (*vide infra*), that detracts from the effective use of cluster self-assembly for nanoelectronics.

The chain length of the alkanedithiol coupling agent and the shell thickness of the cluster are important variables in the cluster self-assembly chemistry. To probe the sensitivity of the self-assembly to these variables, a systematic series of four alkanedithiols with carbon atom chain lengths ranging from 6 to 12 is investigated as depicted in Fig. 3. The dithiol coupling agent should be of sufficient length to extend through the shells of adjacent clusters for an efficient deposition but not be excessively long so as to increase the distance of closest approach between adjacent clusters and thereby reduce the probability of electron tunneling. This consideration is illustrated in the sketch in Fig. 3. The $Au:C_6(1:1)$ and $Au:C_2C_6(1:1)$ clusters were selected for this experiment on the basis of having a relatively thin but stable shell and a correspondingly high conductivity ($6 \times 10^{-6}\ \Omega^{-1}\ cm^{-1}$ and $3 \times 10^{-5}\ \Omega^{-1}\ cm^{-1}$, respectively). As such, the current

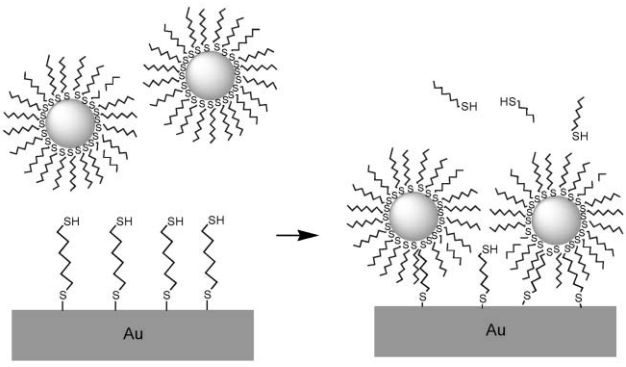

Fig. 2 Sketch depicting self-assembly chemistry used to deposit monolayer encapsulated gold clusters onto a gold electrode surface.

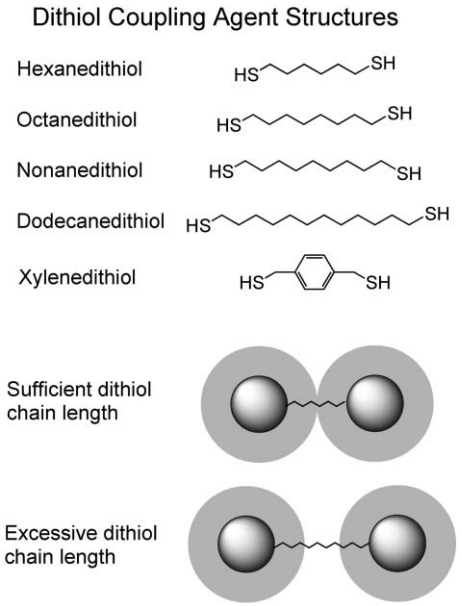

Fig. 3 Depiction of the $Au:C_6(1:1)$ and the $Au:C_2C_6(1:1)$ clusters and the series of dithiol coupling agents.

increments following successive cluster depositions are measurable, and the corresponding shell thicknesses are within the breaching range of the 6 to 12 carbon chain length of the alkanedithiol. Similar experiments are also performed using *p*-xylenedithiol in order to probe the effect of a coupling agent with a similar chain length but different structural rigidity and polarizability.

To study the layer-by-layer self-assembly process by which monolayer-encapsulated gold clusters are deposited onto silicon dioxide and gold electrode surfaces we employ the micron-scale interdigitated electrode device as illustrated in Fig. 1b. Using the micron-scale devices is advantageous for several reasons. First, the gap between the electrode fingers is 15 μm, and this is much more reproducible from device to device than is the nanometre-scale gap. Second, the measured current represents an average over a much larger number of individual clusters so that irregularities due to variation in cluster size or shell junctions (*i.e.* interfaces between adjacent cluster cores) do not cause major perturbations. Finally, the electrode's larger size simplifies both the self-assembly immersion manipulations and the electrical contacting for the current measurement. To attach clusters to the silicon dioxide surface in the electrode gap we activate the surface using a silanethiol coupling agent [(3-mercaptopropyl)trimethoxysilane] as illustrated in Fig. 4. This technique has previously been shown to be an effective way of immobilizing a cluster deposition.[14,17] The deposition of a layer of clusters onto the electrode/substrate is a two-step cycle. In the first step, the surfaces of both the gold electrode and the silicon oxide substrate are activated with the respective dithiol and silanethiol coupling agents. The second step is an immersion in a cluster solution to ideally immobilize a layer of clusters onto the electrode/substrate. If additional layers of clusters are desired, successive deposition cycles are employed. In the first step of a successive cycle the substrate is immersed in a dithiol solution to activate the previous layer of immobilized clusters by a partial exchange reaction of the dithiol with the monothiol ligand. This is followed by an immersion in a cluster solution to deposit an additional layer of clusters. The growth of the cluster film carried out in this way can be monitored by measuring the changes in the conductivity of the film that occur following each deposition cycle. Another way of following the film growth on SiO_2 surfaces, at least in its initial stages, is to monitor the increasing gold-to-silicon ratio using XPS.

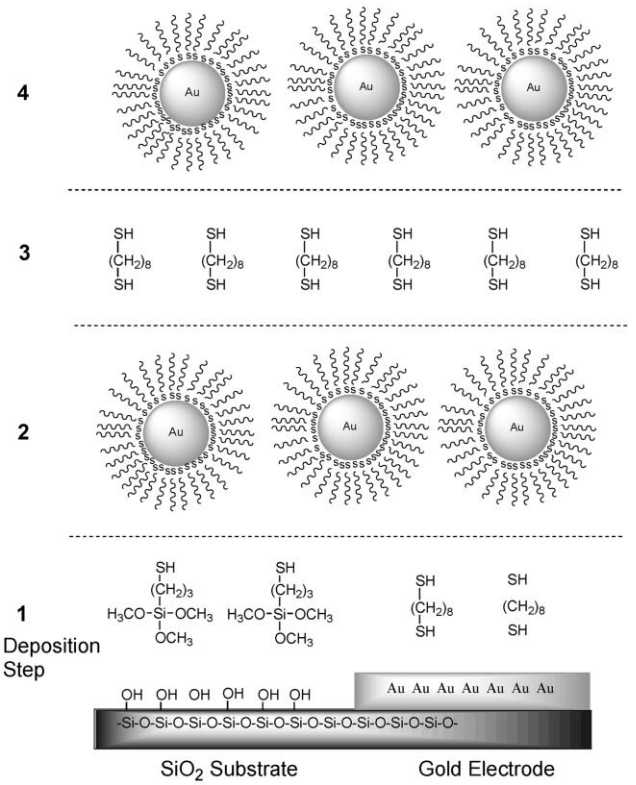

Fig. 4 Sketch depicting the self-assembly chemistry deposition of monolayer encapsulated gold clusters onto the silicon dioxide and gold interdigital electrode surfaces.

Cluster deposition/current measurement

The changes in current that occur during 16 cycles of an octanedithiol–$Au:C_6(1:1)$ deposition are displayed in Fig. 5. These data are obtained by making current measurements on the half cycle (after thiol coupling agent solution immersion) and the full cycle (after $Au:C_6(1:1)$ cluster solution immersion) steps of the deposition. As seen in Fig. 5, significant current is not measured until after 3 or 4 cycles of deposition are completed. This indicates that a fully continuous conducting path is not established until after the third deposition cycle. After this point, further deposition cycles result in an overall current increase but in a pattern where the current increases after the cluster immersion step and partially decreases after the dithiol immersion step. Clearly, the deposition of additional clusters augments the current, while the dithiol immersion diminishes the current. The latter decline in current correlates with evidence (*vide infra*) indicating that the dithiol may

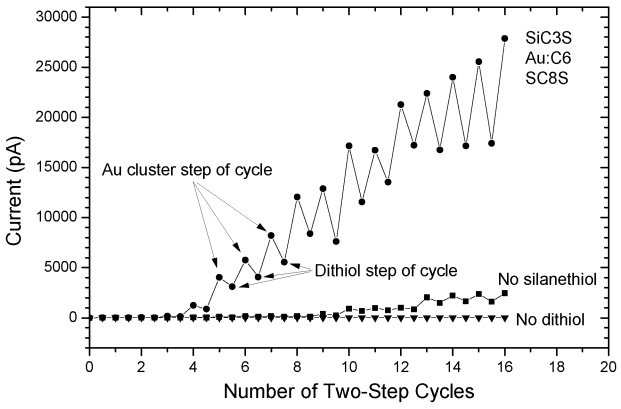

Fig. 5 The changes in current resulting from 16 cycles of an octanedithiol–$Au:C_6(1:1)$ deposition onto the 15 μm interdigital electrode.

sequester a small fraction of the immobilized gold clusters and remove them from the deposition by dissolving them back into solution. An important detail in the deposition procedure is therefore to limit the dithiol immersion to a short time so as to obtain a sufficient exchange with the ligand shell molecules of the outermost clusters but not so long as to effect a significant removal of these clusters. Immersion times for the data obtained in Fig. 5 are 2 minutes which are typical for these depositions and are clearly adequate for film growth. After 10 to 15 deposition cycles, the coating on the electrode and substrate appears to the eye as a transparent film with a very faint tinge of maroon color.

To better understand the role of the alkanedithiol and silanethiol coupling agents, control experiments are conducted in which these agents are individually omitted from the deposition procedure. For these experiments the system of octanedithiol–$Au:C_6(1:1)$ is used and the results are displayed in Fig. 5. In a first control experiment the octanedithiol is used only for the initial activation of the gold electrode surfaces but not in subsequent cycles (*i.e.*, in the first step of each deposition cycle a blank solvent is used). In this situation the silicon dioxide surface between the electrodes receives the activation treatment of silanethiol, and, if the self-assembly chemistry is functioning in an ideal manner, a continuous film of clusters should build up on this surface. However, after 16 cycles of deposition, no detectable current is measured. This indicates that the initial substrate/electrode surface activation does not promote self-assembly of a cluster layer with sufficient continuity to support an electron transport path and that the octanedithiol is essential for coupling subsequent layers to establish an electron transport path across the 15 μm electrode gap. In a second control experiment the silanethiol treatment activating the silicon dioxide surface between the electrodes is not carried out. In this case a detectable and slowly increasing amount of current is observed after 9 deposition cycles (Fig. 5). From this we conclude that a few clusters adsorb at active sites on the silicon dioxide surface despite its not being treated with the silanethiol. These few adsorbed clusters serve as nuclei for the outward growth of subsequent layers of cluster deposition which eventually establish conducting pathways across the electrode gap at a reduced rate.

A third similar control experiment examines the effect of omitting the alkanedithiol activation of the gold electrode surface. In this case nanoscale electrodes are used in place of the micron-scale electrode so that deposition of only a few clusters within the gap would result in measurable current. The SiO_2 surface is not activated with the silanethiol so that cluster deposition is influenced by the presence or omission of alkanedithiol activation of the gold electrode surface, and only a single deposition cycle is performed. The basic finding is that when dithiol was included in the process over 70% of the 35 devices tested show conduction (>1 pA) whereas when it was not included only 10% of the 10 devices tested did. Thus it would appear that the dithiol coupling of the clusters to the electrode is near-essential for good conduction to be established.

Cluster deposition/XPS measurement

The undesired adsorption of a gold cluster on the silicon dioxide surface (*vide supra*) is investigated by XPS control experiments. Simple immersion of a clean SiO_2 coated silicon wafer in the $Au:C_6(1:1)$ cluster solution followed by solvent washing results in gold being adsorbed on the surface as detected by XPS. To quantify the amount, a Langmuir–Blodgett film of the $Au:C_6(1:1)$ cluster transferred to the surface of the wafer was used as a monolayer coverage reference. A four cycle deposition (octanedithiol–$Au:C_6(1:1)$) using a clean SiO_2 surface (untreated with the silanethiol coupling agent) is employed. For comparative purposes, the

Table 1 XPS Analysis of gold cluster–dithiol self-assembly on SiO_2

Deposition	Au : Si ratio
$Au:C_6(1:1)$ LB film	2.4
$Au:C_6(1:1)$/C8dithiol (4 cycles)	0.9–1.9
$Au:C_6(1:1)$/C8dithiol (4 cycles) + sonicate	2.2
$Au:C_6(1:1)$/C8dithiol silanize + 4 cycles	0.054
$Au:C_6(1:1)$/C8dithiol HF treat + 4 cycles	0.049
$Au:C_4(1:1)$/C8dithiol (4 cycles)	8.8
$Au:C_6(1:1)$/C8dithiol (4 cycles)	0.9–1.9
$Au:C_8(1:1)$/C8dithiol (4 cycles)	0.31
$Au:C_{12}(1:1)$/C8dithiol (4 cycles)	0.20

$Au:C4(1:1)$, $Au:C8(1:1)$ and $Au:C12(1:1)$ clusters are also examined to determine if the cluster shell thickness is an important variable. The XPS measurements of the Au : Si ratio for these control depositions are presented in Table 1. There is clearly an absorption affinity and subsequent deposition growth of these gold clusters on the silicon dioxide surface. After the four cycles of deposition, the $Au:C_6(1:1)$ cluster coverage is about two thirds that of a monolayer. This correlates with the second control experiment in the preceding section where an identical deposition resulted in a detectable current flow after a few more cycles of deposition. This undesired cluster adsorption onto the SiO_2 surface is not detached by simple sonication.

To determine whether an alkanedithiol adsorption onto the silicon dioxide plays a role in anomalous cluster adsorption on silicon dioxide, XPS experiments using the octanedithiol and a chlorine tagged alkanethiol are carried out. XPS analysis for sulfur and carbon on a clean silicon dioxide surface treated with a half cycle immersion in the octanedithiol solution is negative but not particularly definitive because sulfur has a very weak signal and carbon is a ubiquitous contaminant. The chlorine tagged alkanethiol provides a much more sensitive diagnostic than sulfur in the XPS analysis and is used as a surrogate for the octanedithiol in this experiment. Analysis of clean silicon oxide surface treated with a half cycle immersion in a 6-chlorohexane-1-thiol solution detected neither chlorine nor sulfur. This indicates that the alkanethiol adsorption affinity for the silicon dioxide surface is substantially weaker than that of the gold cluster and that it probably plays no role in the undesired adsorption of the gold cluster onto the silicon dioxide surface.

Based on these results, we speculate that there are "active sites" in the silicon dioxide surface to which the monolayer protected gold cluster has an affinity for adsorption. These "active sites" are believed to be non-specific in nature except for a bias toward high surface energy adsorbates. The XPS data in Table 1 for the cluster series $Au:C_n(1:1)$ $n = 4, 6, 8, 12$ show an inverse correlation of deposition with ligand shell thickness. The gold core surface is relatively high in surface energy and, if not sufficiently protected by a ligand shell, would be attracted to an active site in the silicon dioxide surface. The butanethiol ligand shell offers little protection, and a high level of adsorption is observed. In the case of the $Au:C_6(1:1)$ cluster we observe that sonication is unsuccessful in removing the clusters (see Table 1) which indicates that the bonding to the silicon dioxide surface is reasonably strong. The longer chain (8 and 12 carbon atoms) alkanethiols of the ligand shell are effective in diminishing this undesired interaction and thereby decreasing the adsorption. The thickness of the ligand shell is thus an important factor in cluster deposition surface selectivity and an important design parameter if gold nanocluster self-assembly is to be utilized in fabrication of nanoelectronic devices.

Passivating the SiO_2 surface by silanizing reagents or by a hydrogen fluoride treatment improves resistance to undesired

cluster deposition (Table 1). Use of a trichlorosilyl terminated silicone oligomer (Glassclad 6C, Hulls) improves the resistance by a factor of 30. Converting the silicon dioxide surface to an hydrogen terminated silicon by immersion in a HF solution has a near equivalent effect. These two treatments can reduce the gold cluster adsorption, as measured by XPS to about 2% of a monolayer.

Cluster deposition/time dependence

As indicated earlier, the time dependence of both steps in the deposition cycle are important variables in the control of the deposition. Ideally, after the first cycle, the duration of the dithiol activation step should be no longer than that needed for enough dithiol–monothiol exchanges to occur to activate the surface for the cluster deposition step of the cycle. Measurements of current changes resulting from four cycles of octanedithiol–$Au:C_6(1:1)$ starting at the onset of significant current development are depicted in Fig. 6. In this case the dithiol step consists of a 2 min immersion followed by a 12 min immersion in the $Au:C_6(1:1)$ solution with current measurements made at various time intervals during the 14 min. At the end of each 2 min dithiol immersion (16, 30 and 44 min) there is a decrease in current similar to that observed in Fig. 5. Following this dithiol immersion step, current measurements were made initially at half min intervals during the $Au:C_6(1:1)$ solution immersion step. The current rises over the first 2 min of immersion to a value that remains relatively constant over the remaining 10 min of this immersion step. This indicates that the cluster self-assembly is a rapid process for this particular system and that a 2 min $Au:C_6(1:1)$ solution immersion time is sufficient since the increase in current beyond this time interval is nominal.

An optimum dithiol immersion time is a little less easily defined because two processes are involved: substitution of dithiol for the monothiol on the outer cluster deposition layer and sequestering of entire clusters of the outer layer back into solution. The latter process is better illustrated by a control experiment employing a monofunctional alkanethiol in place of the dithiol. After several cycles of the octanedithiol–$Au:C_6(1:1)$ deposition are performed to build up an easily measurable current, the device is immersed in a solution of hexanethiol in place of the octanedithiol, and the current is measured as a function of immersion time for 22 min. The results of this experiment are also depicted in Fig. 6 as the final portion of the current *vs.* time plot. There is a very rapid decrease in the current which levels off to a value approaching zero. This experiment demonstrates the reversibility of the cluster deposition as well as the ligand exchange reaction. It also accounts for the drop in current during the alkanedithiol immersion step in the octanedithiol–$Au:C_6(1:1)$ deposition (Fig. 5). In the case where the self-assembled cluster film is immersed in a large excess of dithiol, many of the dithiol coupling agents are bound only to a single cluster and effectively act as a monofunctional ligand to disperse individual clusters. Thus, in the deposition cycle it is necessary to limit the time for the dithiol immersion step to allow sufficient substitution to accommodate the next cluster deposition step, but not so much substitution that a significant fraction of clusters deposited in the previous step are removed. For the octanedithiol–$Au:C_6(1:1)$ system deposition depicted in Fig. 5 the two minute octanedithiol immersion appears to be a good compromise. One interesting by-product of these observations is that immersion in a concentrated solution of monofunctional alkanethiol might be used to remove the self-assembled cluster deposition thereby regenerating the substrate for additional experiments.

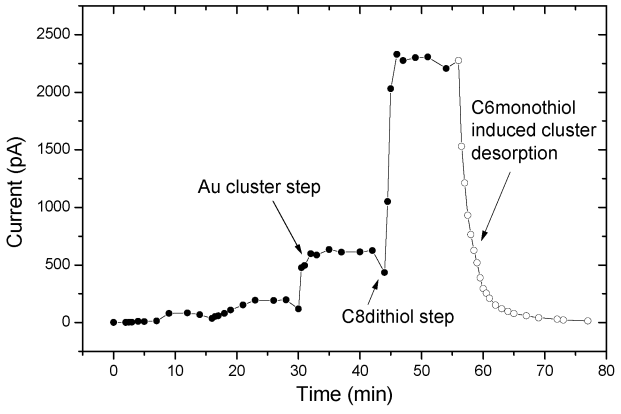

Fig. 6 Time dependence of 15 μm interdigital electrode current changes resulting from four cycles of octanedithiol and $Au:C_6(1:1)$ deposition steps starting at the onset of significant current development (●) and from immersion into a hexanethiol solution (○).

Dithiol chain length dependence

The alkanedithiol chain length is varied from 6 to 12 carbon atoms, and its effect on the measured current during 16 cycles of deposition with the $Au:C_6(1:1)$ cluster is presented in Fig. 7. Two general types of behavior are observed. The octanedithiol and *p*-xylenedithiol display significant current increases with deposition cycle while the hexanedithiol, nonanedithiol and dodecanedithiol display only modest increases. In the progression of a 6, 8, 9 and 12 carbon alkanedithiol, it appears that the chain length corresponding to 8 methylene groups represents an optimum for electron transport. As discussed above in the chemical system design section, two aspects of the alkanedithiol chain length were conjectured to be important for electron transport in these self-assembled cluster films: a sufficient length to span the thicknesses of two adjacent clusters' ligand shells, and a lack of excessive length so that the bonding of the coupling agent does not increase the separation between the gold core surfaces of adjacent clusters. These considerations may be applied to the interpretation of the data of Fig. 7. The hexanedithiol appears to have too short a chain length to efficiently link clusters in the self-assembly reaction. The nonanedithiol and dodecanedithiol instead appear to have an efficient self-assembly chemistry but show reduced conductivity because their extra chain length results in a decreased tunneling probability. This electron transport reduction with increasing dithiol chain length correlates well with measurements reported for self-assembled films of alkanedithiols and bare gold clusters.[14]

The early deposition data (cycles 1 through 6) of Fig. 7 display some interesting features, and an expanded plot of this region is presented in Fig. 8. At the first deposition cycle, the longer alkanedithiols (nonane and dodecane) produce a

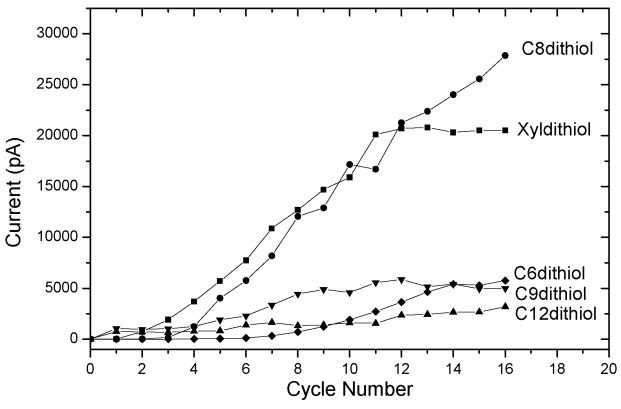

Fig. 7 The changes in current resulting from 16 cycles of deposition of the $Au:C_6(1:1)$ cluster onto the 15 μm interdigital electrode using dithiols of varying chain length.

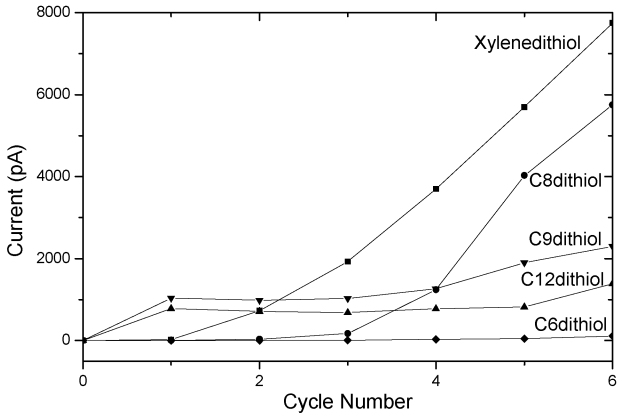

Fig. 8 Expanded view of the current response data to the initial six deposition cycles of the $Au:C_6(1:1)$ cluster onto the 15 μm interdigital electrode using dithiols of varying chain length.

significantly higher level of conduction than do the shorter dithiols. This first cycle of deposition is uniquely different from succeeding ones in that the alkanedithiol adsorbs onto the clean electrode surface in the first step which is then followed by a coupling to the surface to the monolayer encapsulated core of the $Au:C_6(1:1)$ cluster in the second step. As such, the alkanedithiol's bonding and orientation on the gold electrode surface are important issues for self-assembly reaction with the first layer of clusters. We expect that the efficiency of coupling the cluster to the electrode surface correlates with the chain length, bonding and orientation of the alkanedithiol in the self-assembled monolayer on this surface. With some dependence on chain length, alkanedithiol monolayers have been reported to bond to gold surfaces with one or both thiol groups and to orient in an upright, flat or looped position.[18] In the absence of a good study of a homologous series of alkanedithiol monolayers, the trend this literature appears to indicate is that: short chain length dithiols (hexanedithiol) form well ordered monolayers where both thiol groups bond to the surface and the chain is parallel to the surface;[18h] intermediate chain length dithiols (octanedithiol, nonanedithiol) form monolayers where thiol group bonding and chain orientation are similar to that of the short chain dithiols[18c–f] and/or where one thiol group bonds to the surface and the chain is oriented upright to the surface with the second thiol group projecting outward;[18b,18g,18i] Long chain length dithiols (dodecanedithiol) form less ordered monolayers where the bonding involves both thiol groups with the chain in a looped conformation[18g,18j] and/or a single thiol group with the chain extending outward.[18a] The results for conductivity in Fig. 8 after the first cycle of deposition are consistent with the longer alkanedithiols being adsorbed onto the gold electrode surface with an orientation that promotes a more efficient coupling with the $Au:C_6(1:1)$ cluster. An efficient coupling would be favored by the dithiol adsorbed onto the electrode with its chain normal to the surface and a single thiol group extending outward.

Successive cycles of deposition require a dithiol coupling between adjacent clusters whose core surfaces are previously complexed with monofunctional alkanethiols. The conductance data in Fig. 8 display a crossover after 2 to 4 cycles of deposition where the intermediate chain length alkanedithiols promote higher conductances. As described above, this correlates with a sufficient but not excessive length for an efficient electron transport. The short chain length hexanedithiol lacks a sufficient length to effectively span the thickness of two shells of adjacent clusters.

The efficiency of the cluster–cluster coupling reaction may also be assessed by XPS measurements of the deposition using the variable chain length dithiols. In this case the substrate is a blank silicon dioxide coated wafer which is first treated with the

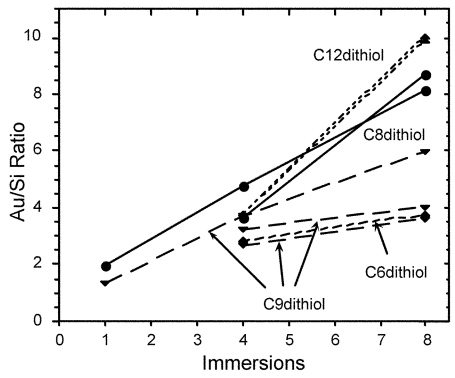

Fig. 9 XPS measurements of the Au : Si ratio after 1, 4 and 8 cycles of alkanedithiol–$Au:C_6(1:1)$ deposition onto a silicon dioxide surface using the 6, 8, 9, and 12 carbon dithiols.

(3-mercaptopropyl)trimethoxysilane coupling agent. Measurements of the Au : Si ratio were made after 4 and 8 cycles of alkanedithiol–$Au:C_6(1:1)$ deposition using the same 6, 8, 9, and 12 carbon dithiols as in the electrical measurement. The results are presented in Fig. 9. In agreement with the current measurements of Figs. 7 and 8, the hexanedithiol displays the least efficiency in the self-assembly reaction, and the octane- and dodecanedithiols display the high efficiencies. The nonanedithiol is an apparent outlier despite three attempts at this measurement. It may be there is something unique about this dithiol, and this issue is currently under study.

Aromatic structural effects

The effect of placing an aromatic structure in either or both the gold cluster ligand shell and the dithiol coupling agent is investigated using the $Au:C_2C_6(1:1)$ cluster in place of the $Au:C_6(1:1)$ cluster and the *p*-xylenedithiol in place of the octanedithiol. As indicated in the 'Chemical system design' section, this substitution has nominal effect on the dimensions of ligand shell thickness and coupling agent chain length, but the phenylene ring is a much more polarizable and rigid. The effect of this substitution on the electron transport during 16 cycles of deposition is presented in Fig. 10. Comparing the octanedithiol–$Au:C_2C_6(1:1)$ with the octanedithiol–$Au:C_6(1:1)$ system, the increment in current with deposition cycle is enhanced by almost a factor of two. This higher conductivity correlates with an aromatic structure in the shell lowering the average barrier between clusters. When the aromatic structure is only in the coupling agent as in the *p*-xylenedithiol–$Au:C_6(1:1)$ system, the increases in current with deposition do

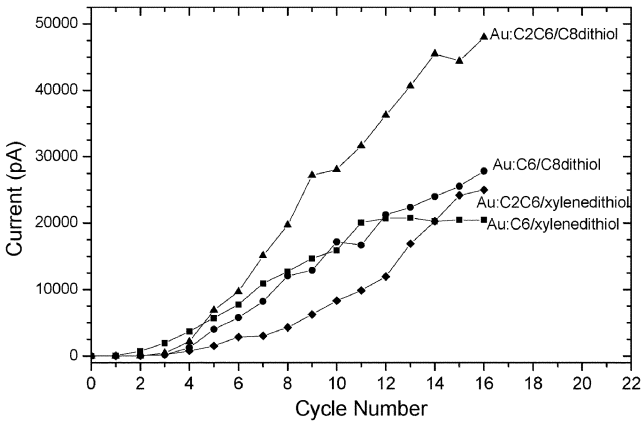

Fig. 10 Comparison of the current response changes resulting from deposition of the $Au:C_6(1:1)$ and $Au:C_2C_6(1:1)$ clusters with the octanedithiol and xylenedithiol coupling agents in various combinations of self-assembly onto the 15 μm interdigital electrode.

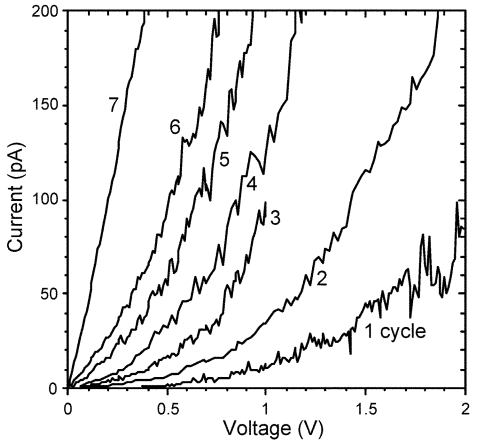

Fig. 11 Current–voltage characteristics for a nanoscale device with a gap spacing of 20 nm and a width of 50 nm as a function of the number of deposition cycles of $AuC_6(1:1)$.

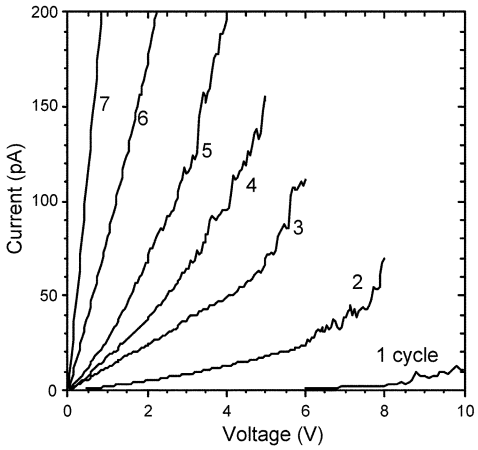

Fig. 12 The same as Fig. 11 but for a nanoscale device with a gap spacing of 50 nm.

not differ much from the all-aliphatic system until a leveling off occurs after the twelfth cycle. When the system is the all aromatic *p*-xylenedithiol–$Au:C_2C_6$ (1 : 1) system, the current increments are initially lower but eventually increase to attain a current level nearly equivalent to the octanedithiol–$Au:C_6(1:1)$ aliphatic analog after 16 cycles of deposition. It would appear that the *p*-xylenedithiol coupling agent is less effective at coupling clusters and thereby promoting electron transport.

Nanoscale electrode deposition/current measurement

The same deposition processes described earlier and used on the micron-scale devices are readily applied at nanometre scales. To see this, we focus on the nonanedithiol–$Au:C_6(1:1)$ system since Fig. 7 indicates that this will exhibit appreciable conduction even after a single layer of deposition. In Fig. 11, we plot the current–voltage characteristics of a nanoscale device after each deposition cycle up to 6 cycles. This device had a gap spacing of 20 nm and a width of 50 nm and, because of geometrical considerations, the current levels are much smaller than were observed in the micron-scale devices. As expected, current is observed after the initial cycle and it increases monotonically as more clusters are deposited. Most interesting in this plot is that the transport after the first cycle is strongly nonlinear but it becomes increasingly ohmic as additional cycles are completed. In a more detailed study[8a] we explored the nonlinear *I–V* behavior of a cluster monolayer in nanoscale devices. Based on its temperature, gap width and core size dependences and on comparison with numerical simulations, we concluded that the observed nonlinearity was primarily due to Coulomb blockade effects. Adding more layers (Fig. 11) then opens up more unblockaded channels for conduction and leads to the ohmic behavior that we observe. One final observation comes from a similar set of data, shown in Fig. 12, for a nanoscale device which had a similar width but a significantly larger gap spacing (50 nm). Here, the *I–V* characteristics during the first few deposition cycles exhibit *both* Coulomb blockade-associated nonlinearity and ohmic behavior. The reason is that, because of the larger gap, the threshold voltage associated with the Coulomb blockade is substantially larger and in the low voltage regime where the current is mostly blockaded we are thus able to see a build-up of an ohmic background associated with the sheet conductance of the unblockaded paths across the entire cluster film.

Summary

The utilization of self-assembly chemistry for the fabrication of electronic devices from gold nanoclusters requires control and tradeoff of molecular structures, reaction conditions and scale of substrate features. The results of this work illustrate that alkanethiol stabilized gold clusters in combination with alkanedithiol coupling agents can be used for such purposes. However, considerations of the efficiencies of the self-assembled deposition and of the electron transport need to be properly balanced. Of specific importance are the chain length of the alkanedithiol coupling agent relative to that of the alkanethiol in the ligand shell and the time dependence of the dithiol coupling agent exchange reaction to establish sufficient substitution for deposition of successive cluster layers. For the case of the $Au:C_6(1:1)$ cluster, we find that alkanedithiols of 8 or 9 methylene groups have sufficient chain lengths for an efficient self-assembly and that longer chain lengths strongly reduce the efficiency of electron transport. To observe and possibly utilize Coulomb blockade effects displayed by nanocluster depositions, the size of the cluster and the number of clusters involved in the electron transport must be small. This requires clusters with core sizes on the order of 1 to 2 nm, only 1 or 2 layers of cluster deposition and gaps of 50 nm or less between substrate features making contact with the cluster deposition.

Acknowledgement

The Office of Naval Research is gratefully acknowledged for financial support.

References

1 (*a*) H. Wohltjen and A. W. Snow, *Anal. Chem.*, 1998, **70**, 2856; (*b*) A. N. Shipway, M. Lahav, R. Blonder and I. Willner, *Chem. Mater.*, 1999, **11**, 13; (*c*) A. B. Kharitonov, A. N. Shipway and I. Willner, *Anal. Chem.*, 1999, **71**, 5441; (*d*) M. Lahav, R. Gabai, A. N. Shipway and I. Willner, *Chem. Commun.*, 1999, 1937; (*e*) S. D. Evans, S. R. Johnson, Y. L. Cheng and T. Shen, *J. Mater. Chem.*, 2000, **10**, 183; (*f*) M. Lahav, A. N. Shipway, I. Willner, M. B. Nielsen and J. F. Stoddart, *J. Electroanal. Chem.*, 2000, **482**, 217; (*g*) A. Labande and D. Astruc, *Chem. Commun.*, 2000, 1007.

2 (*a*) M. Dorogi, J. Gomez, R. Osifchin, R. P. Andres and R. Reifenberger, *Phys. Rev. B*, 1995, **52**, 9071; (*b*) R. P. Andres, T. Bein, M. Dorogi, S. Feng, J. I. Henderson, C. P. Kubiak, W. Mahoney, R. G. Osifchin and R. Reifenberger, *Science*, 1996, **272**, 1323; (*c*) R. P. Andres, S. Datta, M. Dorogi, J. Gomez, J. Henderson, D. B. Janes, V. R. Kolagunta, C. P. Kubiak, W. Mahoney, R. F. Osifichin, R. Reifenberger, M. P. Samanta and W. Tian, *J. Vac. Sci. Technol. A*, 1996, **14**, 1178.

3 R. S. Ingram, M. J. Hostetler, R. W. Murray, T. G. Schaaff, J. T. Khoury, R. L. Whetten, T. P. Bigioni, D. K. Guthrie and P. N. First, *J. Am. Chem. Soc.*, 1997, **119**, 9279.

4 S. Chen, R. S. Ingram, M. J. Hostetler, J. J. Pietron, R. W. Murray, T. G. Schaaff, J. T. Khoury, M. M. Alvarez and R. L. Whetten, *Science*, 1998, **280**, 2098.

5 L. C. Brousseau III, Q. Zhao, D. A. Schultz and D. L. Feldheim, *J. Am. Chem. Soc.*, 1998, **120**, 7645.
6 (*a*) D. B. Janes, V. R. Kolagunta, R. G. Osifchin, J. D. Bielefeld, R. P. Andres, J. I. Henderson and C. P. Kubiak, *Superlattices Microstruct.*, 1995, **18**, 275; (*b*) D. L. Klein, P. L. McEuan, J. E. B. Katari, R. Roth and A. P. Alivisatos, *Appl. Phys. Lett.*, 1996, **68**, 2574; (*c*) T. Sato and H. Ahmed, *Appl. Phys. Lett.*, 1997, **70**, 2759; (*d*) T. Sato, H. Ahmed, D. Brown and B. F. G. Johnson, *Appl.Phys.*, 1997, **82**, 696; (*e*) N. Fishelson, I. Shkrob, O. Lev, J. Gun and A. D. Modestov, *Langmuir*, 2001, **17**, 403; (*f*) T. Ogawa, K. Kobayashi, G. Masuda, T. Takase and S. Maeda, *Thin Solid Films*, 2001, **393**, 374.
7 A. N. Shipway, E. Katz and I. Willner, *ChemPhysChem*, 2000, **1**, 18.
8 (*a*) M. G. Ancona, W. Kruppa, R. W. Rendell, A. W. Snow, D. Park and J. B. Boos, *Phys. Rev. B*, 2001, **64**, 3408; (*b*) A. W. Snow, M. G. Ancona, W. Kruppa, D. Park, J. B. Boos and G. G. Jernigan, *Mater. Res. Soc. Symp. Proc.*, 1999, **582**, H12.5.1.
9 H. Wohltjen, W. R. Barger, A. W. Snow and N. L. Jarvis, *IEEE Trans. Electron. Devices*, 1985, **ED-32**(7), 1170.
10 (*a*) A. W. Snow and H. Wohltjen, *Chem. Mater.*, 1998, **10**, 947; (*b*) M. J. Hostetler, J. E. Wingate, C.-J. Zhong, J. E. Harris, R. W. Vachet, .R. Clark M, J. D. Londono, S. J. Green, J. J. Stokes, G. D. Wignall, G. L. Glish, M. D. Porter, N. D. Evans and R. W. Murray, *Langmuir*, 1998, **14**, 17.
11 M. Brust, M. Walker, D. Bethell, D. J. Schiffrin and R. Whyman, *J. Chem. Soc., Chem. Commun.*, 1994, 801.
12 S. Chen and R. W. Murray, *Langmuir*, 1999, **15**, 682.
13 G. G. Urquhart, J. W. Gates Jr. and R. Connor, *Org. Synth.*, 1955, **Coll. Vol. III**, 363.
14 (*a*) D. Bethell, M. Brust, D. J. Schiffrin and C. Kiely, *J. Electroanal. Chem.*, 1996, **409**, 137; (*b*) M. Brust, R. Etchenique, E. J. Calvo and G. J. Gordillo, *Chem. Commun.*, 1996, 1949; (*c*) M. Brust, D. Bethell, C. J. Kiely and D. J. Schrffrin, *Langmuir*, 1998, **14**, 5425.
15 (*a*) M. D. Musick, C. D. Keating, M. H. Keefe and M. J. Natan, *Chem. Mater.*, 1997, **9**, 1499; (*b*) M. D. Musick, C. D. Keating, A. Lyon, S. L. Botsko, D. J. Pena, W. D. Holliway, T. M. McEvoy, J. N. Richardson and M. J. Natan, *Chem. Mater.*, 2000, **12**, 2869; (*c*) N. Fishelson, O. L. Sckrob, J. Gun and A. D. Modestov, *Langmuir*, 2001, **17**, 403; (*d*) L. Han, M. M. Maye, F. L. Leibowitz, N. K. Ly and C. J. Zhong, *J. Mater. Chem.*, 2001, **11**, 1258.
16 (*a*) R. L. Whetten, J. T. Khoury, M. M. Alvarez, S. Murthy, I. Vezmar, Z. L. Wang, P. W. Stephens, C. L. Cleveland, W. D. Luedke and U. Landman, *Adv. Mater.*, 1996, **8**, 428; (*b*) N. Z. Clarke, C. Waters, K. A. Johnson, J. Satherley and D. Schiffrin, *Langmuir*, 2001, **17**, 6048.
17 K. C. Grabar, R. G. Freeman, M. B. Hommer and M. J. Natan, *Anal. Chem.*, 1995, **67**, 735.
18 (*a*) T. Nakamura, H. Kondoh, M. Matsumoto and H. Nozoye, *Langmuir*, 1996, **12**, 5977; (*b*) H. Rieley, G. K. Kendall, F. W. Zemicael, T. L. Smith and S. Yang, *Langmuir*, 1998, **14**, 5147; (*c*) K. Kobayashi, J. Umemura, T. Horiuchi, H. Yamada and K. Matsushige, *Jpn. J. Appl. Phys.*, 1998, **37**, L297; (*d*) P. Kohli, K. K. Taylor, J. J. Harris and G. J. Blanchard, *J. Am. Chem. Soc.*, 1998, **120**, 11962; (*e*) K. Kobayashi, T. Horiuchi, H. Yamada and K. Matsushige, *Thin Solid Films*, 1998, **331**, 210; (*f*) K. Kobayashi, H. Yamada, T. Horiuchi and K. Matsushige, *Appl. Surf. Sci.*, 1999, **144–145**, 435; (*g*) C. Winter, U. Weckenmann, R. A. Fischer, J. Käshammer, V. Scheumann and S. Mittler, *Chem. Vap. Deposition*, 2000, **6**, 199; (*h*) T. Y. B. Leung, M. C. Gerstenberg, D. J. Lavrich and G. Scoles, *Langmuir*, 2000, **16**, 549; (*i*) W. Deng, D. Fujita, L. Yang, H. Nejo and C. Bai, *Jpn. J. Appl. Phys.*, 2000, **39**, L751; (*j*) A.-S. Duwez, G. Pfister-Guillouzo, J. Delhalle and J. Riga, *J. Phys. Chem. B*, 2000, **104**, 9029.